ELSEVIER

Journal of Alloys and Compounds 262–263 (1997) 134–140

Journal of ALLOYS AND COMPOUNDS

Relationship between the structural and the magnetic properties of $ErMn_{12-x}Fe_x$ compounds

M. Morales[a,*], M. Artigas[b], M. Bacmann[a], D. Fruchart[a], J.L. Soubeyroux[a], P. Wolfers[a]

[a] *Laboratoire de Cristallographie, CNRS, BP 166, 38042 Grenoble Cédex 9, France*
[b] *Instituto de Ciencia de Materiales de Aragon, CSIC, 50009 Zaragoza, Spain*

Abstract

The crystal and magnetic properties of intermetallic compounds of formula $ErMn_{12-x}Fe_x$ with $x = 0, 2, 4, 6, 8$, have been analysed versus the relative distribution of the transition metal (Mn or Fe) on the different *d*-metal sites of the tetragonal structure. Neutron diffraction and magnetisation measurements allow better understanding of the relationships between the atom ordering and the (Mn,Fe)–(Mn,Fe), (Mn,Fe)–Er and Er–Er magnetic couplings. © 1997 Elsevier Science S.A.

Keywords: Ferromagnetic alloys; Crystal structure; Magnetisation; Magnetic couplings

1. Introduction

During the last few decades, it has been found that several intermetallic compounds of rare earth elements (R) and 3*d*-transition metals can be used as starting materials for permanent magnets of outstanding properties [1]. In particular, insertion of light elements such as H, C, or N in iron-rich alloys of $ThMn_{12}$ type leads to compounds exhibiting high values of Curie temperature, saturation magnetisation and magnetocrystalline anisotropy [2]. The compounds RFe_{12} do not exist, but they can be stabilised by alloying of selected 3*d*, 4*d*, Al, Si... elements sharing less electron density than Fe. Contrarily to the Fe-rich compounds, the RMn_{12} alloys mostly exhibit antiferromagnetic ordering, taking place at low temperature [3,4]. A complex magnetic behaviour should result in ferromagnetic to antiferromagnetic competing interactions supported by the 3*d*–3*d* and 3*d*–R contributions to exchange. In this paper, we present the results of neutron diffraction studies and systematic magnetisation measurements along the dilution of Mn by Fe in the solid solutions $ErMn_{12-x}Fe_x$ ($0 \leq x \leq 8$).

2. Experimental

The alloys were prepared by induction melting of the metal constituents in a water-cooled copper crucible under a purified argon atmosphere. The samples where checked by X-ray powder diffraction for phase purity. In some cases, small amounts of β-manganese (Mn-rich side) and $Er_6(Mn,Fe)_{23}$ were detected. The neutron powder diffraction experiments were performed at ILL, Grenoble, France, using a high-resolution D2B diffractometer with $\lambda = 1.594$ Å and a D1B position-sensitive detector with $\lambda = 2.522$ Å. With the former, diffraction patterns were recorded at room temperature where only nuclear scattering was observed. Then the magnetic contributions to diffraction were analysed from 1.5 to 300 K by using the latter diffractometer. Magnetisation measurements on powder samples were carried out by means of an automated extraction magnetometer equipped with a cryomagnet that provides fields up to 10 T.

* Corresponding author.

0925-8388/97/$17.00
PII S0925-8388(97)00369-1

3. Results

3.1. Crystal structure analysis

From the X-rays and the high resolution neutron diffraction patterns (D2B), all the samples were found to crystallise in the $ThMn_{12}$ type of structure [5] which belongs to the SG I4/mmm with $Z = 2$. The Er atom occupies the $2a$ Wyckoff position, whereas the transition metal atoms occupy the $8i$, $8j$ and $8f$ positions. Rietveld's type refinements were carried out with the FULLPROF program [6]. It was assumed that each of the $3d$ metal sites is fully occupied by iron and manganese atoms. Consequently the iron to manganese ratio was not constrained to the nominal stoichiometry of the starting materials.

For example, the observed neutron diffraction pattern of $ErMn_8Fe_4$ and the calculated Rietveld refinement profile are shown in Fig. 1.

The a cell parameter decreases linearly from $x = 0$ to $x = 8$ whereas the c-cell parameter remains almost constant (Fig. 2). As a result of this behaviour, the unit cell volume decreases linearly with x at a slope of approx. 1.0 Å^3/Fe. The smaller atomic volume of Fe (11.77 Å^3) in comparison with Mn (12.8 Å^3) could explain this decrease.

For each of the $ErMn_{12-x}Fe_x$ compounds, the refined Fe content (x_{ref}) and its distribution in the three transition metal sites $8i$, $8j$, $8f$ are shown in Table 1. In Fig. 3, these iron occupation numbers are compared with those expected in the case of a random Mn to Fe distribution represented by a diagonal line. It can be seen that it is nearly the case for the $8j$ site only. A marked preference for the occupation of the $8f$ site by iron is observed whereas the manganese atoms exhibit a pronounced proclivity for the $8i$ site occupation.

The selected ordering of M elements for iron in the $Nd_2Fe_{14}B$, R_2Fe_{17} and $R(Fe,M)_{12}$ series have been

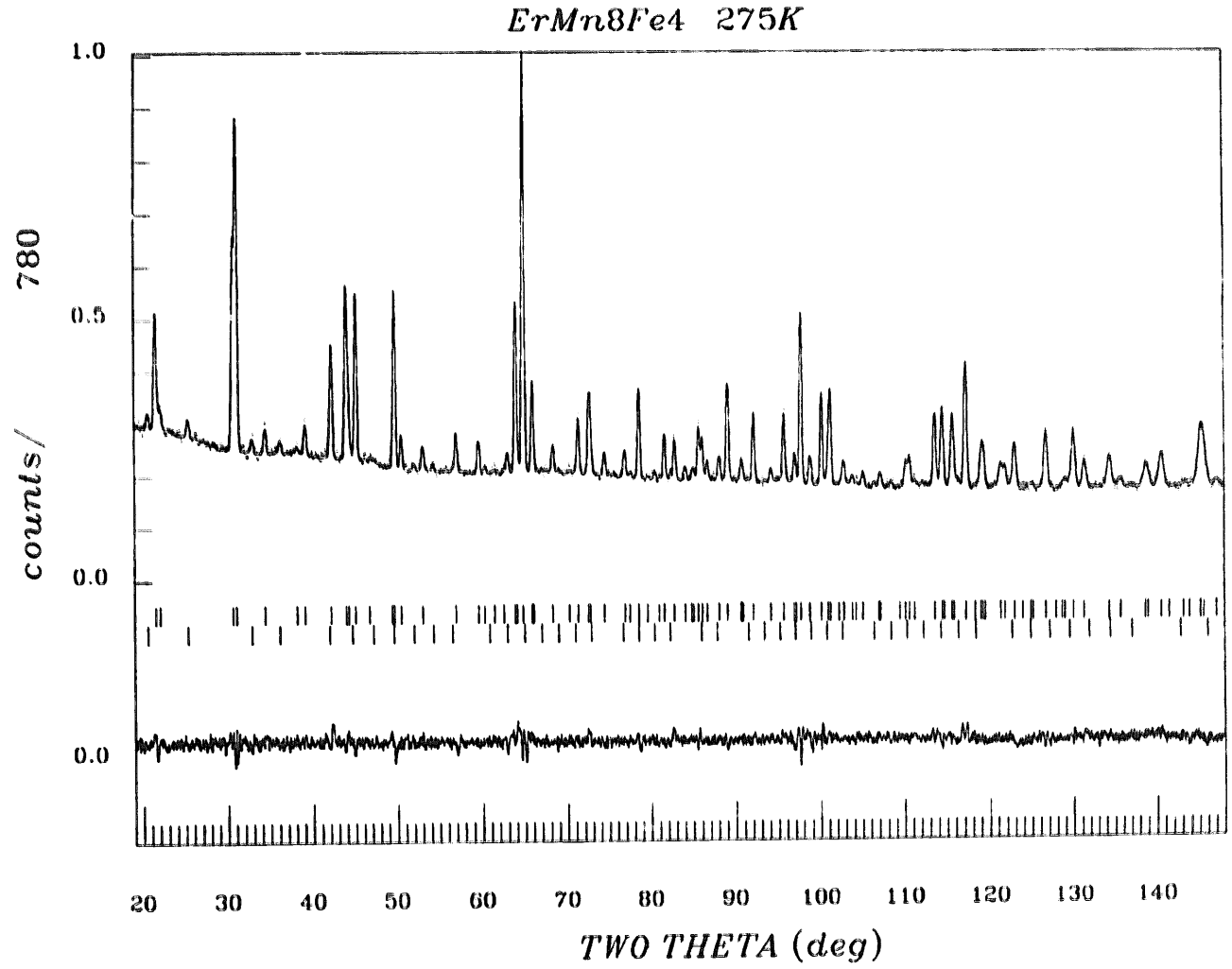

Fig. 1. Observed, calculated and difference neutron patterns. Vertical bars indicate Bragg peak positions for $ErMn_8Fe_4$ and β-Mn, respectively.

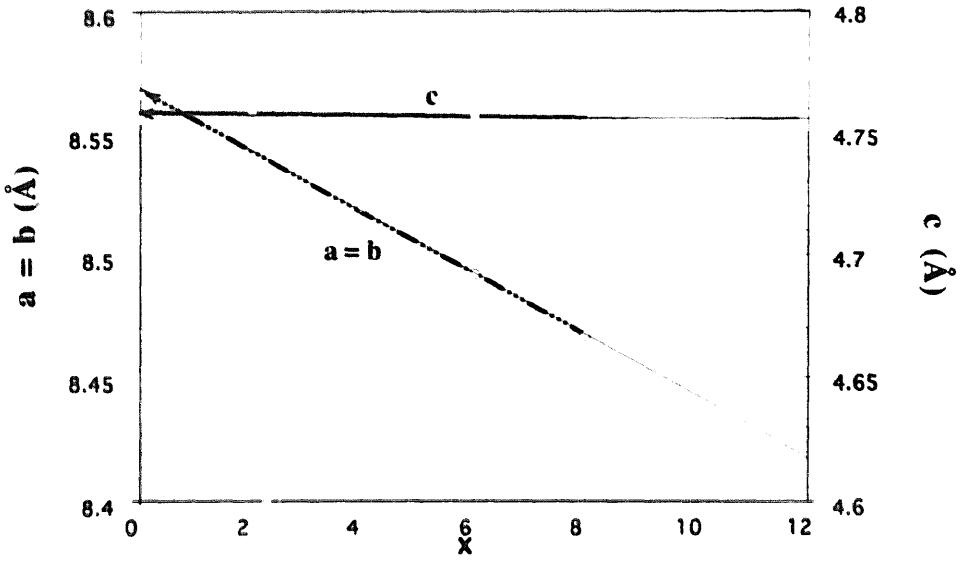

Fig. 2. The a and c-cell parameter variations vs. x.

Table 1
Distribution of the Fe content on the three transition metal sites $8i$, $8j$ and $8f$

x	x_{refi}	Fe occupation %		
		$8i$	$8j$	$8f$
2	2.13(2)	5.4(3)	17.4(2)	30.6(2)
4	4.04(2)	8.5(2)	35.4(2)	57.0(2)
6	5.98(3)	18.4(2)	56.4(3)	74.7(3)
8	7.85(3)	35.2(2)	74.7(3)	86.4(3)

explained in terms of an interplay between atomic size and enthalpy considerations [1]. In the case of $Er(Mn,Fe)_{12}$ solid solutions, the enthalpies of mixing between rare earth and manganese or iron metal do not differ significantly. Size effects would select the substituting atoms with the largest radius and the low d-electron concentration to the positions corresponding to the largest Voronoi polyhedra. In the $ErMn_{12}$ structure the volume relation $V(8i) > V(8j) > V(8f)$ is observed between these polyhedra [7]. For all compositions, the experimental results show that the iron/manganese atom distribution on the three $3d$ sites agrees with the atomic size consideration. The poor affinity of iron to populate the $8i$ site is consistent with the fact that RFe_{12} compounds do not exist.

3.2. Magnetic properties

Isotherm (0–10 T) and isofield under 0.1 T (1.7–300

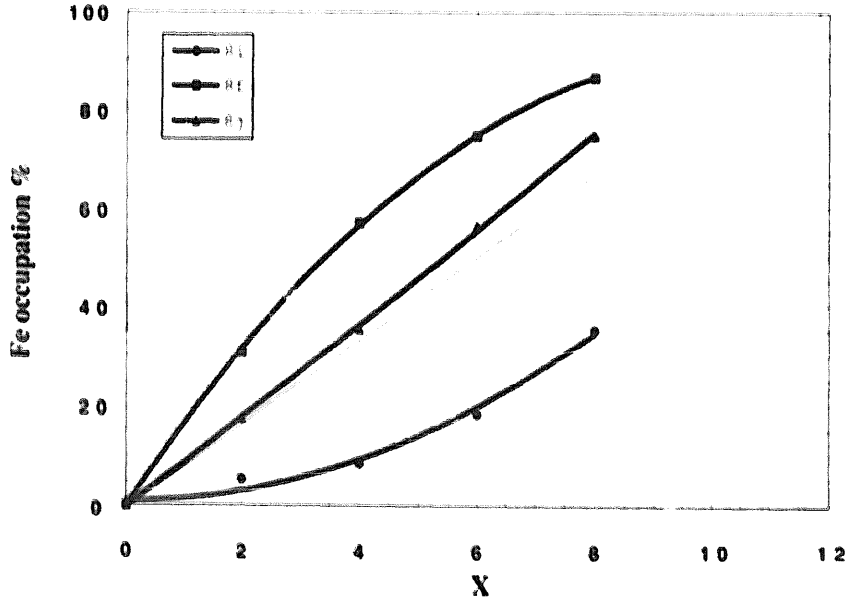

Fig. 3. Fe atoms occupation of the three sites $8i$, $8j$ and $8f$.

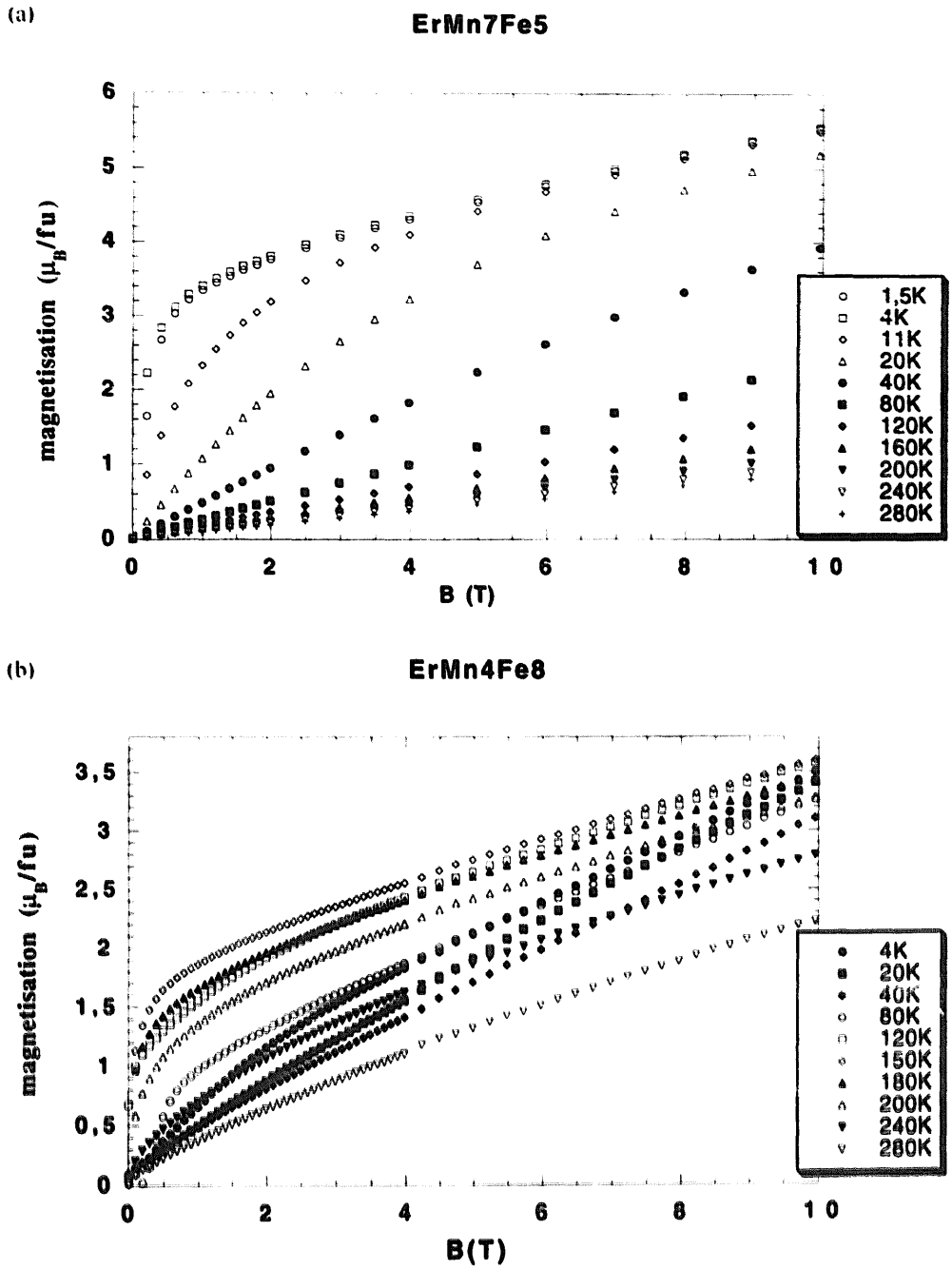

Fig. 4. (a) Magnetisation curves for $ErMn_7Fe_5$. (b) Magnetisation curves for $ErMn_4Fe_8$.

K) magnetisation measurements have been recorded on compositions given above and on additional samples with $x = 5$ and 7. From $x = 0$–6, a ferromagnetic component has been shown to take place down to ≈ 15 K (Fig. 4a). For intermediate temperatures, the magnetisation curves correspond to antiferromagnetic behaviour. For the iron-rich side ($x = 7$ and 8), the very low temperature magnetisation is markedly reduced in comparison with the previous samples (Fig. 4b), but the susceptibility is maximum close to 150 K where the extrapolated magnetisation lies approximately between 0.8 and 1.9 μ_B/f.u. The 1.7 K magnetisation curve ($x = 7$) plotted vs. field reveals a step-by-step increase in the polarisation that should indicate some equilibrium between competing interactions (Fig. 5). Moreover, the isotherm magnetisation curves does not follow a continuous succession vs. temperature (Brillouin-like behaviour) (Fig. 4b).

For compositions ranging close to $x = 5$ and 6, zero-field cooling (ZFC) and field cooled (FC under $H = 0.1$ T) magnetisation curves, show clear-cut indications of a spin glass like behaviour (Fig. 6).

3.3. Magnetic structure determination

The magnetic configurations related to each site of

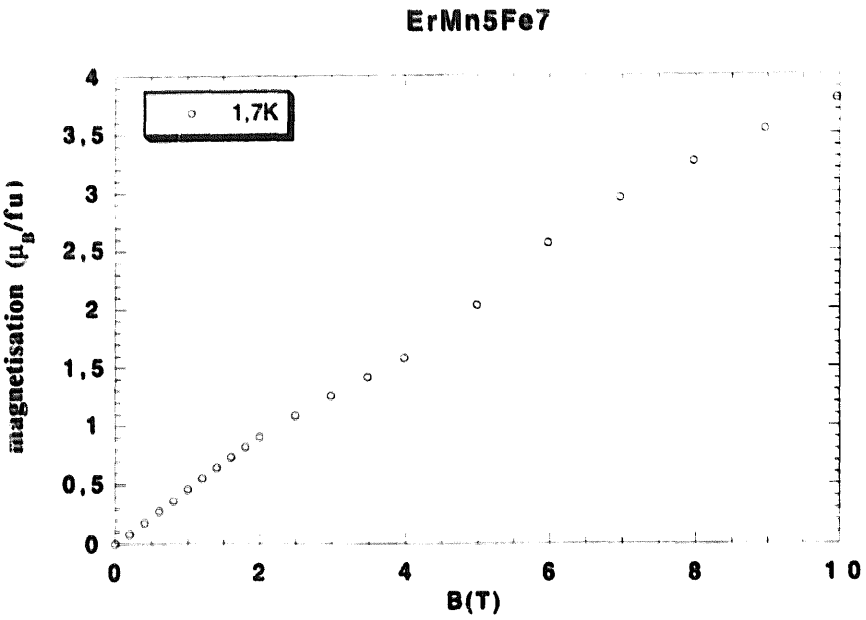

Fig. 5. Magnetisation curve at $T = 1.7$ K for $ErMn_5Fe_7$.

the metal sublattices have been deduced from neutron diffraction data recorded in the 2–300 K temperature range using the D1B diffractometer. High statistics patterns have been recorded at 2, 19, 300 K, and temperature-resolved experiments have been done in the whole range of temperature to follow the thermal variations of the magnetic reflections. At room temperature only nuclear scattering is detected whereas at $T = 2$ K and 19 K we observe new diffraction lines for all the studied compositions. They can be indexed from the crystal unit cell under the condition $h + k + l = 2n + 1$, consequently magnetic moments corresponding to translation I are antiparallel. From the thermal variations of these lines, the ordering temperatures have been deduced. They are reported in Table 2 and a maximum of the Néel temperature T_N is found for $x \approx 6$. This result is consistent with those of the electrical resistivity measurements performed on the $RMn_{12-x}Fe_x$ series with R = Y, Gd, Tb, Dy, Ho [8].

Depending on composition and temperature, a second set of magnetic contributions appears on the nuclear peaks and can be related to the ferromagnetic component observed on the magnetisation curves. For

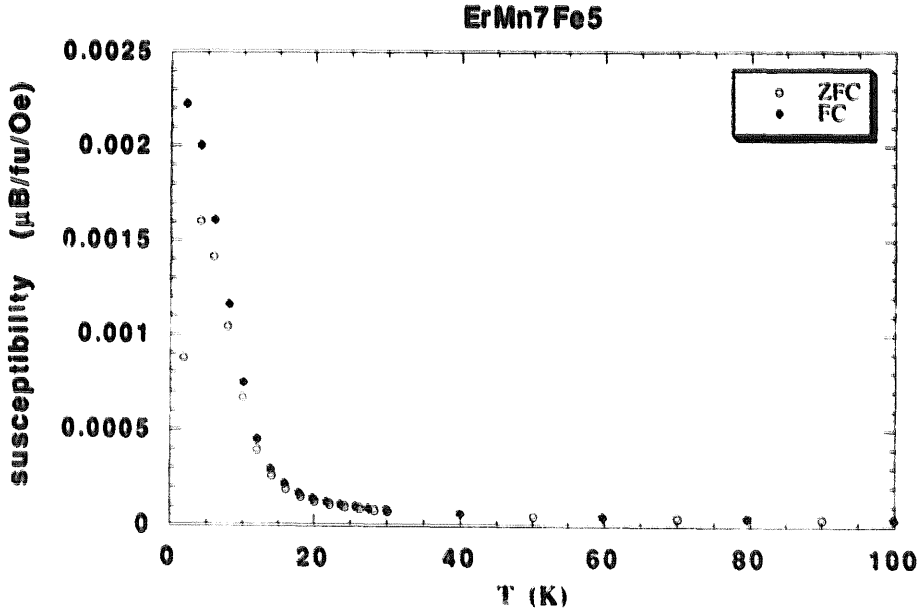

Fig. 6. Isofield magnetisation curves under $H = 0.1$ T for $ErMn_7Fe_5$.

Table 2
Ordering temperatures T_N and T_C in $ErMn_{12-x}Fe_x$ compounds as determined by neutron diffraction

x	0	2	6	8
T_N	80 K	170 K	220 K	200 K
T_C	4 K	4 K	14 K	146 K

$0 \leq x \leq 6$, only the low temperature diffraction patterns exhibit such contributions, whereas for $x = 8$ they are observed up to $T \approx 150$ K but are far weaker. Analysis of their thermal variation allows us to determine T_C the Curie temperature values Table 2.

To determine the magnetic structures in the light of the neutron diffraction data, considerations of group theory analysis (GTA) were applied [9]. Pertinent details of this procedure will be reported later. The basis vectors related to the 8*i*, 8*j*, 8*f* and 2*a* sites are given in Table 3 only for the eight one-dimension irreducible representations of the SG I4/mmm in the case $\chi[I] = -1$. Comparison of the experimental data with those calculated based on the GTA allows us to select the linear combinations of the Γ_{3u} representation at $T = 19$ K for $0 \leq x \leq 6$. The corresponding model represented in Fig. 7 leads to a complex non-collinear antiferromagnetic structure on the 3*d* metal sites in the (*a*,*b*) plane, but no moment is observed for the Er one. For the same compounds, but at $T = 2$ K, a ferromagnetic component attributed to erbium and lying along the *c*-axis is superimposed onto the 3*d* antiferromagnetic system.

For the iron-rich side ($x = 8$) with respect to the magnetisation measurements, changes in the magnetic arrangements are evidenced at 2 and 19 K with the occurrence of ferrimagnetism related to the 3*d*

Table 3
Basis vectors related to the 8*i*, 8*j*, 8*f* and 2*a* sites of I4/mmm ($\chi[I] = -1$) corresponding to the eight one-dimension irreducible representations

	8*i*, 8*j*		8*f*		2*a*
	x, y	z	x, y	z	x, y z
Γ_{1e}					
Γ_{2e}		$F_{1,4}$			$S_1 - S_2$
Γ_{3e}					
Γ_{4e}		$C_{1,4}$			
Γ_{1u}	$S_{1x} - S_{2x} + S_{3x} - S_{4x}$		$A_{(1,4)x} + G_{(1,4)x}$	$F_{1,4}$	
Γ_{2u}	$S_{1x} - S_{2x} - S_{3x} + S_{4x}$		$A_{(1,4)x} - G_{(1,4)x}$		
Γ_{3u}	$S_{1x} - S_{2x} - S_{3x} + S_{4x}$		$G_{(1,4)x} - A_{(1,4)x}$		
Γ_{4u}	$S_{1x} - S_{2x} + S_{3x} - S_{4x}$		$G_{(1,4)x} + A_{(1,4)x}$	$C_{1,4}$	

Notes: The atoms are numbered in the order of the International Tables of Crystallography Vol I. For the 8*i*, 8*j* and 8*f* sites the given basis vectors only related to four atoms (1–4) must be completed by the same but antiparallel arrangement related to the four missing atoms (5–8).
F = + + + +, G = + − + −, C = + + − −, A = + − − +.

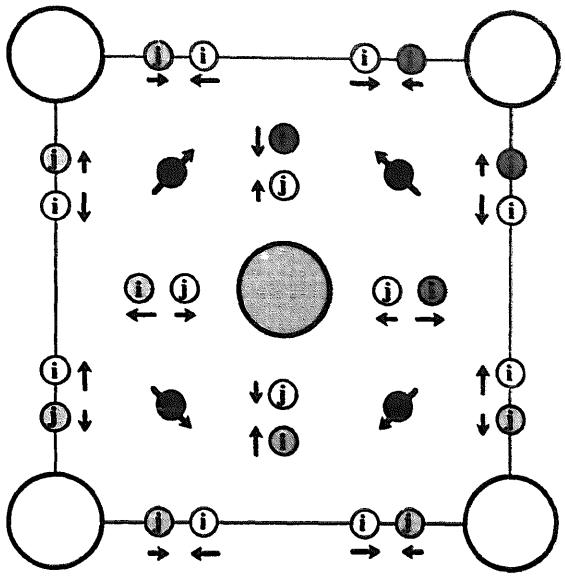

Fig. 7. Magnetic structure in the (*a*, *b*) plane for the $ErMn_{12-x}Fe_x$ compounds with $0 \leq x \leq 6$ at $T = 19$ K. The 3*d* atoms in 8*f* positions are represented by full circles ($z = 1/4$, 3/4). Erbium atoms are represented by large circles and (Mn, Fe) atoms by small circles; atoms drawn with open circles lie in the plane $z = 0$, those with grey circles in the plane $z = 1/2$ and those with black circles in the plane $z = 1/4$ and $z = 3/4$.

(8*j*, 8*f*) and R sites. Weak magnetisation results from the antiparallel components ($\approx 0.2\mu_B$/f.u.) and the previously described AF components still remain on the 8*i* and 8*j* sites.

All the refined magnetic components found by using the MXD program [10] are reported in Table 4 and correspond to excellent reliability factors not exceeding 3%.

For $0 \leq x \leq 6$ the substitution of Mn by Fe leads to an increase of the magnetic moment on the 8*i* site. This variation is consistent with the evolution of the Néel temperature. On the other hand the moment values on 8*j* and 8*f* sites remain very weak.

Table 4
Refined magnetic components in μ_B for $ErMn_{12-x}Fe_x$ compounds at $T = 2$ K and 19 K

		8*i*	8*j*		8*f*		2*a*
		x, y	x, y	z	x, y	z	z
$x = 0$	2 K	−0.76(1)	0.38(1)		0.47(1)		6.0(4)
	19 K	−0.67(1)	0.37(1)		0.48(1)		
$x = 2$	2 K	−1.55(2)	0.02(1)		0.22(1)		2.5(3)
	19 K	−1.66(2)	0.05(11)		0.22(8)		
$x = 4$	2 K	−1.8(1)	0.62(9)		0.64(7)		0
$x = 6$	2 K	−1.98(5)	0.57(4)		0.50(7)		5.3(1)
	19 K	−1.65(6)	0.87(5)		0.92(7)		
$x = 8$	2 K	−1.10(4)	0.40(4)	−0.77(8)		−0.97(5)	7.1(1)
	19 K	−1.10(1)	0.39(4)	−0.75(1)		−1.01(7)	6.8(1)

The antiferromagnetic arrangement of the (Mn,Fe) moments gives evidence for negative interactions depending strongly on distance. Because of the symmetry of the antiferromagnetic structure, Er-(Mn,Fe) interactions cancel on the Er site. The effects of the crystal field on the rare earth atoms are stronger than the exchange interactions.

4. Conclusion

Experimental results show that in the $ErMn_{12-x}Fe_x$ ($0 \leq x \leq 8$) compounds, two ordering temperatures are observed, the higher one corresponding to mainly antiferromagnetic interactions within the $3d$ sublattices, the much lower one revealing a ferromagnetic ordering between erbium atoms. The low temperature magnetisation measurements show that the former interactions are much stronger than the latter, thus an incomplete ferromagnetic ordering with a spin glass like behaviour takes place at low temperature on the R-sublattice for intermediate x values.

References

[1] K.H.J. Buschow, D.B. de Mooij, in: I.V. Mitchell, J.M.D. Coey, D. Givord (Eds.), Concerted European Action on Magnets (CEAM), Elsevier Applied Science, 1989, pp. 63–75.
[2] E. Tomey, Doctorat Thesis, Grenoble University, 1994.
[3] J. Deportes, D. Givord, Solid State Commun. 19 (1976) 845.
[4] J. Deportes, D. Givord, R. Lemaire, H. Nagai, Physica B 86/88 (1977) 69.
[5] J.V. Florio, R.E. Rundle, A.I. Snow, Acta Crystallogr. 9 (1956) 367–372.
[6] J. Rodriguez-Carvajal, in: XVth Conf. Int. Union of Crystallography, Proceedings of the Satellite Meeting on Powder Diffraction, Toulouse, France, 1990.
[7] M. Artigas, M. Bacmann, D. Fruchart, M. Morales, E. Tomey, ECN'S 96, Physica B (1997) in press.
[8] Y. Amako, S. Saoka, H. Yoshie, H. Nagai, K. Adachi, J. Phys. Soc. Jpn. 64 (1995) 1860.
[9] E.F. Bertaut, Acta Crystallogr. A 24 (1968) 217.
[10] P. Wolfers, J. Appl. Crystallogr. 23 (1990) 554.